Shedding Light on Cerium (III/IV), The Unsung Hero, and Mitigating its Reactive Innocence with Ni

Antonysamy Dennyson Savariraj[a] P.Justin Jesuraj[b], Periyasamy Sivakumar[a], Jilly James[c], Kandasamy Prabakar[d], Hyun Jung[a*].

[a] Advanced Functional Nanohybrid Material Laboratory, Department of Chemistry, Dongguk University Seoul-Campus, Jung-gu, Seoul 04620, Republic of Korea.

[b] Center of Excellence in Materials for Advanced Technologies (CeMAT), Department of Physics and Nanotechnology, SRM Institute of Science and Technology, Kattankulathur 603203, India.

[c] Department of Chemistry, Alphonsa College, Arunapuram P.O, Pala 686 574, Kottayam Dist. Kerala, India.

[d] Advanced Sustainable Energy Laboratory, Department of Electrical and Electronics Engineering, Pusan National University, 2, Busandaehak-ro 36beon-gil, Geumjeong-gu, 46241, Republic of Korea.

*Corresponding Author: chemphile@dongguk.edu (Hyun Jung)

1. Experimental:

1.1 Chemicals

For this research work, nickel nitrate hexahydrate ($Ni(NO_3)_2.6H_2O$), ammonium cerium (IV) nitrate ($(NH_4)_2[Ce(NO_3)_6]$), N-methyl-2-pyrrolidone (NMP), and potassium hydroxide (KOH) were procured from Sigma-Aldrich (South Korea). Carbon black and polyvinylidene fluoride (PVDF) were purchased from Alfa-Aesar (South Korea), while ethanol (99.8%) and acetone (99.8%) were procured from Daejung Chemicals & Metals (South Korea). For the synthesis, all the chemicals and solvents were used without further purification. For the substrate, nickel foams (NFs) (purity > 99.9%) with 2 mm thickness were obtained from MTI South Korea.

1.2 *In-situ* deposition of CeO_2 on NFs

The NFs were subjected to activation by treating with 10% hydrochloric acid (HCl). The NFs were cut to the dimension of 1x2.5 cm and immersed in 10% hydrochloric acid (HCl) for a period of 15 min. Then HCl was drained, and the NFs were washed continuously with deionized (DI) water (18.3 MΩ cm) until obtaining a neutral pH (~7), followed by rinsing with ethanol and drying at 65^{o}C in a vacuum overnight. The NFs with pretreatment as described above were used for the deposition of CeO_2. For the *in-situ* deposition of CeO_2 on NFs, firstly the NFs were masked with Teflon tape with an exposed area of 1×1 cm, which will be the active area. The NFs with masking were attached to the glass slides with the help of Kapton tape. In a beaker containing 50 mL of DI water, 219.29 mg of $(NH_4)_2[Ce(NO_3)_6]$ was dissolved to have a 8 mM solution of $(NH_4)_2[Ce(NO_3)_6]$ and poured into the Teflon liner. The masked NFs attached to the glass slides are lowered down into the Teflon liner and placed vertically. The Teflon liner was covered, and this setup was kept inside the stainless steel container of the hydrothermal unit, and the

hydrothermal reaction was carried out at 120°C for a period of 8 h. After the completion of the reaction, the reaction mixture in the autoclave was cooled to room temperature. The CeO_2-deposited NFs were detached from the glass slides and rinsed with DI water and ethanol, followed by drying at 65 °C for 15 h in a vacuum. The obtained sample was labeled as NF/C for the simplicity of identification.

1.3 *In-situ* growth of CeO_2/NiOOH/$Ni(OH)_2$ heterostructure

For the *in-situ* deposition of the CeO_2/NiOOH/$Ni(OH)_2$ heterostructure on NFs, the hydrothermal method was carried out in the following manner. This was carried out using $(NH_4)_2[Ce(NO_3)_6]$ and $Ni(NO_3)_2 \cdot 6H_2O$ as the sources of Ce and Ni, respectively, and the molar ratio was varied, such as 1.0:1.0 (8 mM:8 mM), 1.0:2.0 (8 mM:16 mM), and 1.0:3.0 (8 mM:24 mM), to obtain different compositions. The molar concentrations of the reagents were calculated for 50 mL, and for the ease of experimenting, the reagents ($(NH_4)_2$ $[Ce(NO_3)_6]$ and $Ni(NO_3)_2 \cdot 6H_2O$) were dissolved separately in two beakers containing 25 mL of DI water. Then $Ni(NO_3)_2 \cdot 6H_2O$ solution was added slowly in drops to $(NH_4)_2$ $[Ce(NO_3)_6]$ solution and stirred for 25 min to form a uniform growth solution. The growth solution obtained was poured into the Teflon liner, and the masked NFs attached to the glass slides were dropped into it. The Teflon liner was closed and placed in the stainless steel container, and the hydrothermal reaction was carried out for 8 h at 120°C. The hydrothermal was carried out under identical conditions (8 h at 120°C) for different concentration ratios, namely 1:1, 1:2, and 1:3, and labeled as NF/CN-1, NF/CN-2, and NF/CN-3 for easy recognition.

1.4 Structural and Morphological Analysis

The prepared electrodes (NF/C, NF/CN-1, NF/CN-2, and NF/CN-3) were analyzed for their structural properties with the help of X-ray diffraction (XRD, D/max-2400, Rigaku, Ultima IV operated at *40* kV and *30* mA). In addition, X-ray photoelectron spectroscopy (XPS) (NOVA, Axis Technology), operated under Al *Kα* radiation with the internal standard of the C 1*s* peak fixed at 284.6 eV, was used to perform XPS and UPS (Ultraviolet Photoelectron Spectroscopy) analysis. Electron paramagnetic resonance spectroscopy (EPRS) was performed using the JES-X3 Series A-System at 293 K. The surface morphology of the electrodes was examined and recorded using scanning electron microscopy (SEM, JEOL, JSM-6700F), and the in-depth analysis of the morphology of the electrode materials and selected-area electron diffraction (SAED) patterns was carried out using high-resolution transmission electron microscopy (HRTEM) (JEOL JEM-3010, Japan) operated at an acceleration of 200 kV. The presence of the constituent elements was recorded using energy-dispersive X-ray (EDX) elemental mapping and EDX spectra.

1.5 Electrochemical characterization

The electrochemical profiles of all the prepared electrodes (NF/C, NF/CN-1, NF/CN-2, and NF/CN-3) were examined using a VSP Biopotentiostat/galvanostat electrochemical workstation (BioLogic-SP-150e-France) at RT (~2°C). The electrochemical features of the electrodes were analyzed in terms of cyclic voltammetry (CV) at various sweep rates, galvanostatic charge discharge (GCD) at different current densities, and electrochemical impedance spectroscopy (EIS) for the frequency range between 10 mHz and 100 kHz under a sinus amplitude of 10 mV with 0 V bias voltage. For all the electrochemical measurements, a freshly prepared 3 M KOH aqueous solution was used as the electrolyte.

1.6 Fabrications of asymmetric hybrid capacitor (AHC)

With the conclusion drawn from the electrochemical analysis, the NF/CN-2 electrode was considered the best-performing electrode, and therefore it was treated as the positrode for assembling the AHC. For the negatrode, porous carbon nanosheet (PC), prepared as per a published work with some modifications [1], was chosen. Since the NF/CN-2 electrode was binder-free, only the negatrode was coated using the prepared slurry. For the preparation of slurry, 75% of active material (PCN), 20% of conductive material (carbon black), and 5% of binder (PVDF) were ground to have a uniform mixture, to which NMP was added while grinding until achieving a consistent slurry. The prepared slurry was applied to pretreated NFs of 1×1 cm active area with a brush and dried in a vacuum overnight. For the assembly of AHC, both the positrode (NF/CN-2) and negatrode (NF/PC) were kept face-to-face with a Whatman filter paper 42 sandwiched in between them to serve as the spacer. This composition was wetted with 3 M KOH, transferred to a coin cell setup, and pressed using a hydraulic coin cell-crimping machine. The fabricated AHC assembly was used for all the electrochemical examinations.

2. Equations:

Using the information from the GCD curves of all the electrodes under the three-electrode system, the areal capacity (C_a) ($mC\ cm^{-2}$) of the electrodes can be obtained from the following equation.

$$C_a = \frac{I \times \Delta t}{a} \qquad \text{(S1)}$$

Here, I stands for the discharge current (mA), Δt represents the discharge time (s), and a is the active area of the electrode (cm^2).

In addition, the specific capacity (C_s) (A g^{-1}) of each electrode can be calculated by considering the mass of the electrode material using the following equation.

$$C_s = \frac{I \times \Delta t}{m} \quad \text{(S2)}$$

Here, I denotes the discharge current (mA), Δt is the discharge time (s), and m represents the mass of the active electrode material deposited on the electrode (mg).

The specific capacitance (C_{sp}) (F g^{-1}) of the electrodes can be calculated from the following equation.

$$C_{sp} = \frac{I \times \Delta t}{\Delta V \times m} \quad \text{(S3)}$$

Where I denotes the discharge current (mA), Δt stands for the discharge time (s), while ΔV represents the potential window (V), and m is the mass of the active electrode material deposited on the electrode (mg).

The reaction kinetics of the participating electrodes can be obtained by calculating the value of the variable b using the following equation.

$$i = av^b \quad \text{(S4)}$$

$$\log i = \log a + b \log v \quad \text{(S5)}$$

In the above equation (S4 & S5), I represents the current (A), υ is the scan rate (V s^{-1}), and a and b are the variable and the slope obtained.

The contribution from capacitive-controlled and diffusion-controlled mechanisms can be obtained from the following equation.

$$i(V) = K_1 v + K_2 v^{1/2} \quad \text{(S6)}$$

In the above equation (S6), *i(V)* denotes the potential-dependent current, $K_1\upsilon$ represents the surface capacitive contribution, and $K_2\upsilon^{1/2}$ stands for the diffusion-controlled contribution. The equation S6 can be rewritten in the following manner to obtain the values of K_1 and K_2.

$$\frac{i(V)}{v^{1/2}} = K_1 v^{1/2} + K_2 \qquad \text{(S7)}$$

For the better functioning of the two-electrode system and to obtain its maximum potential, perfect mass balance between the positrode and the negatrode should be obtained. The rational calculation to obtain the mass ratio between the positrode and the negatrode can be estimated using the following equation ($q^+ = q^-$).

$$\frac{m_+}{m_-} = \frac{C_- \times \Delta V_-}{C_+ \times \Delta V_+} \qquad \text{(S8)}$$

Here 'm_+' and 'm_-' represent the mass of the electrode material on the positrode and the negatrode, respectively, while 'C_+' and 'C-' denote the specific capacity of the positrode and the negatrode, respectively, and 'ΔV_+' and 'ΔV_-' stand for the voltage window of the positrode and the negatrode, respectively.

The specific power (E_s) and specific power (P_s) are the important parameters of an asymmetric hybrid device, and these parameters can be determined using the following equations (S9 and S10).

$$E_s = \frac{I \times \int V(t)dt}{m \times 3.6} \qquad \text{(S9)}$$

$$P_s = \frac{E_s \times 3600}{t} \quad \text{(S10)}$$

Here, E_s denotes the specific energy (Wh kg^{-1}), P_s stands for specific power (W kg^{-1}), and $\int V(t)dt$ stands for the integral area of the GCD curve.

3. Figures and Table

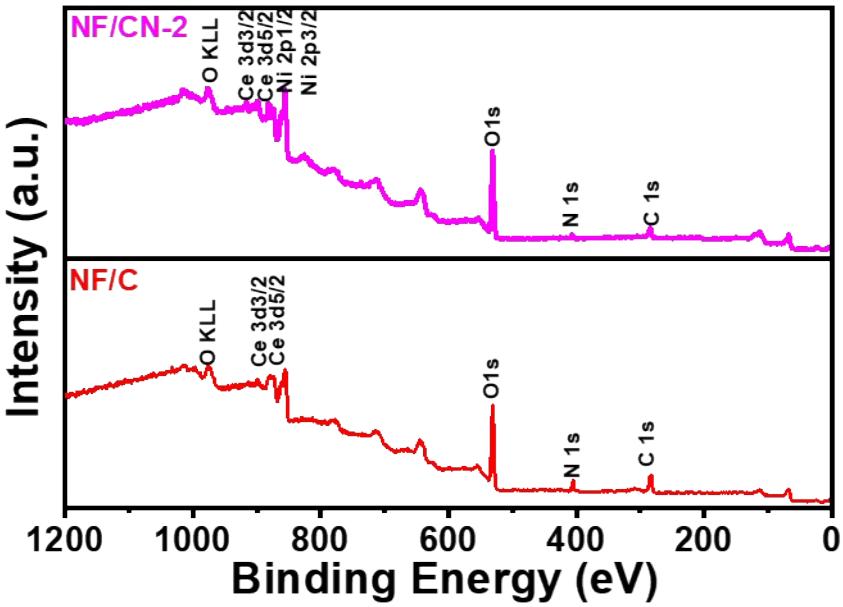

Figure S1. XPS survey spectra of the NF/C and the NF/CN-2 electrodes.

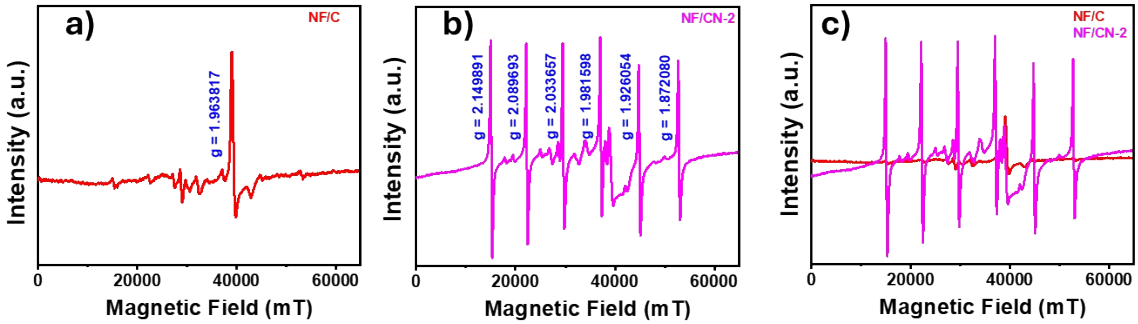

Figure S2. EPRS signals of (a) NF/C, (b) NF/CN-2 electrodes, and (c) a comparison graph of NF/C and NF/CN-2 electrodes.

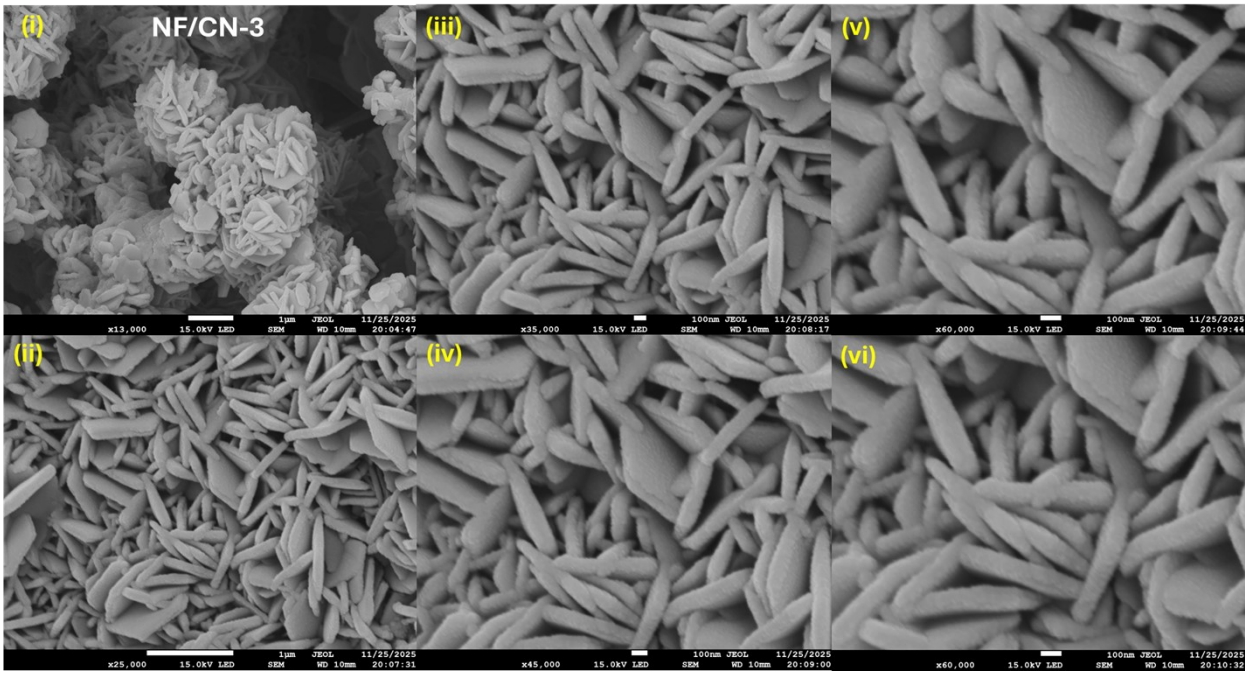

Figure S3. The SEM images of the NF/CN-3 electrode at different magnifications.

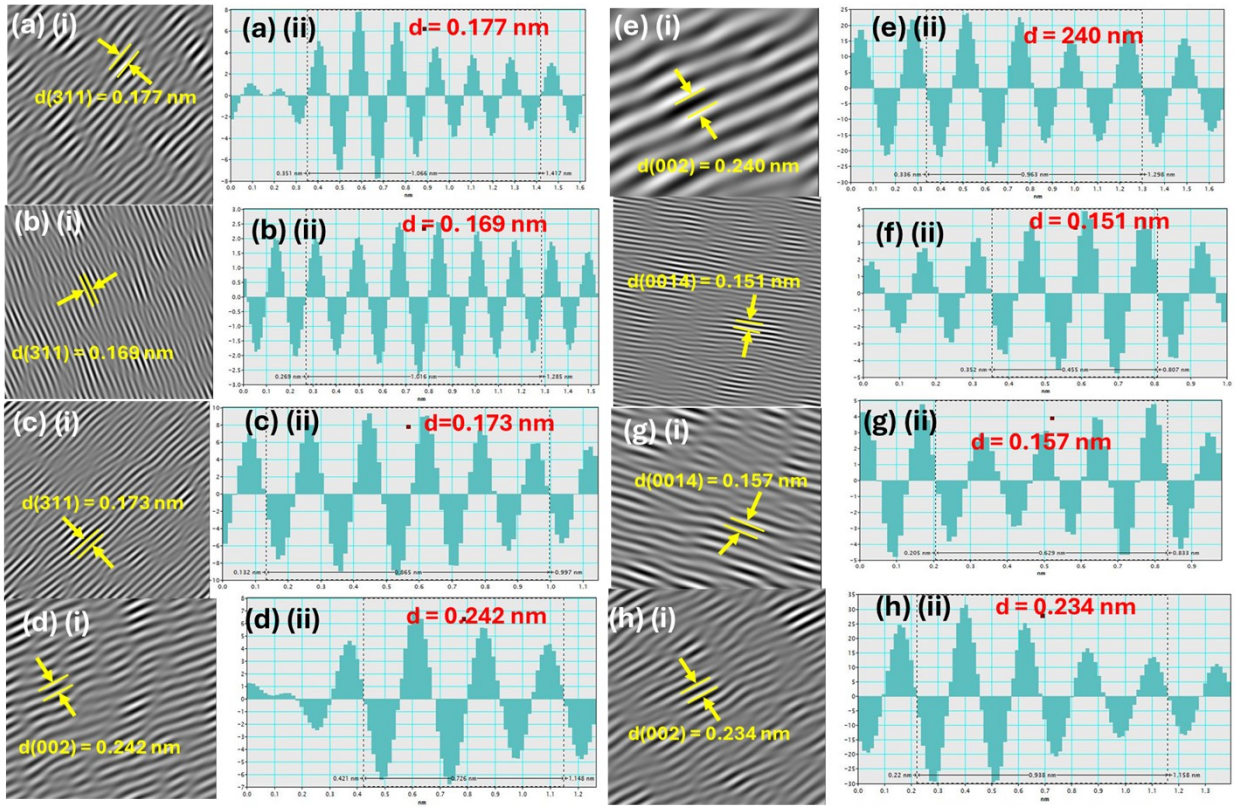

Figure S4. Interplanar fringe spacing measurement carried out for NF/C, NF/CN-1, and NF/CN-2 electrodes.

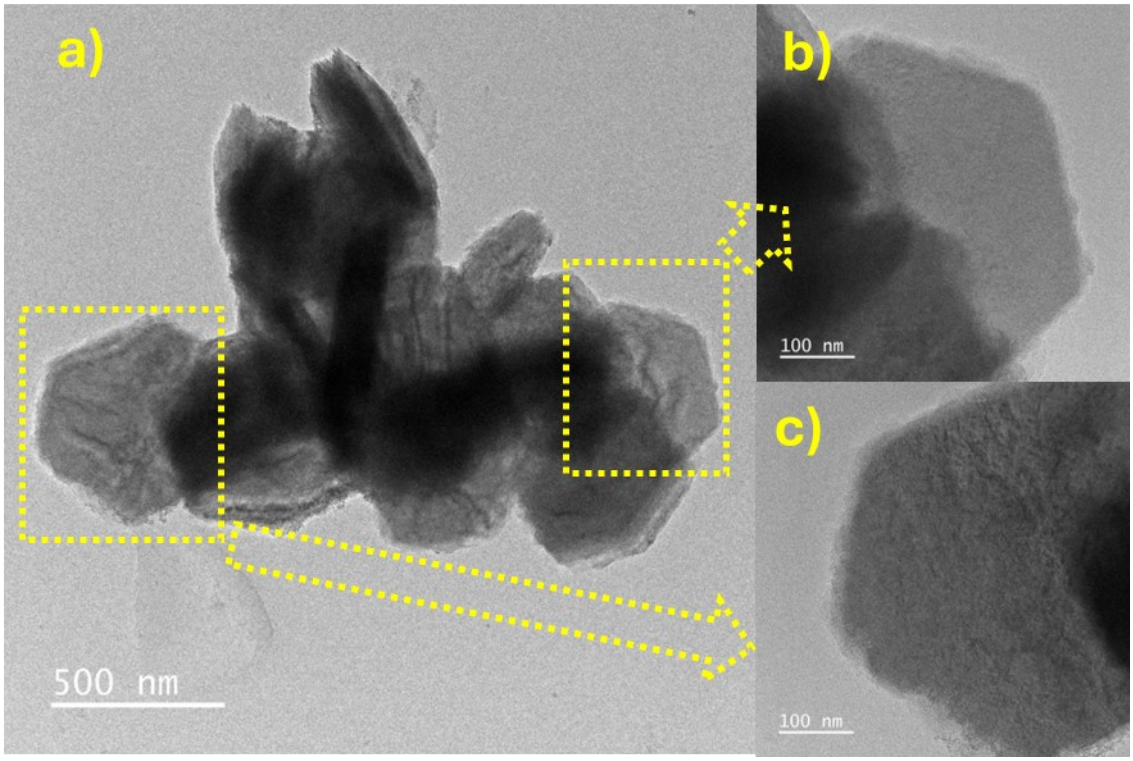

Figure S5. The HR-TEM images of NF/CN-2 electrodes at different magnifications.

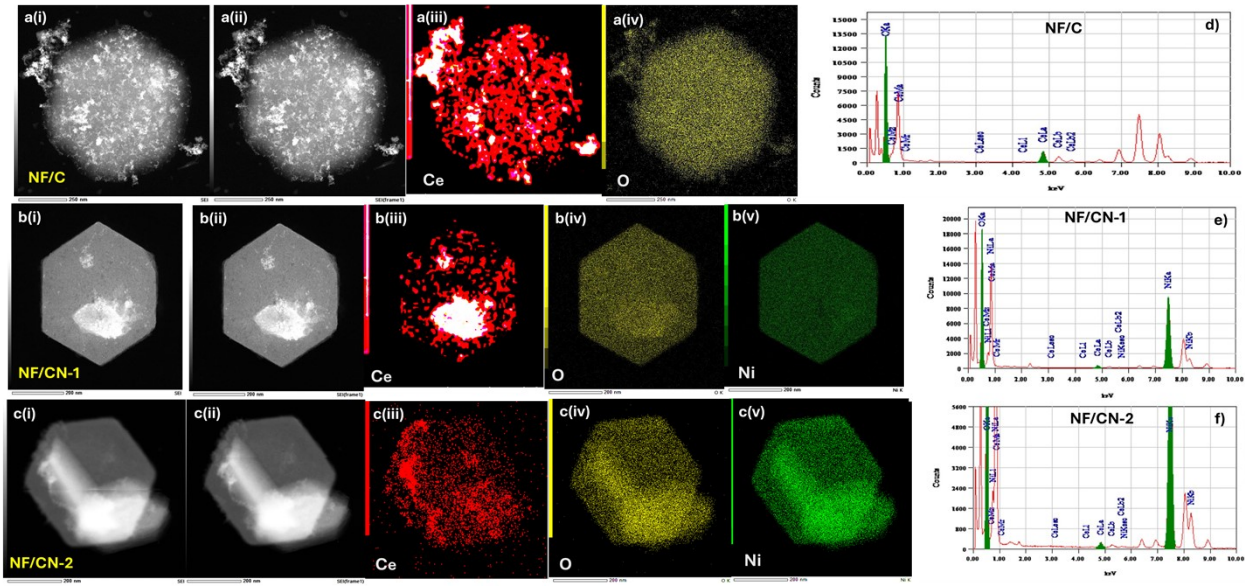

Figure S6. HR-TEM EDX elemental mapping of (a) NF/C, (b) NF/CN-1, and (c) NF/CN-2 electrodes, and energy-dispersive X-ray (EDX) spectra of (d) NF/C, (e) NF/CN-1, and (f) NF/CN-2 electrodes.

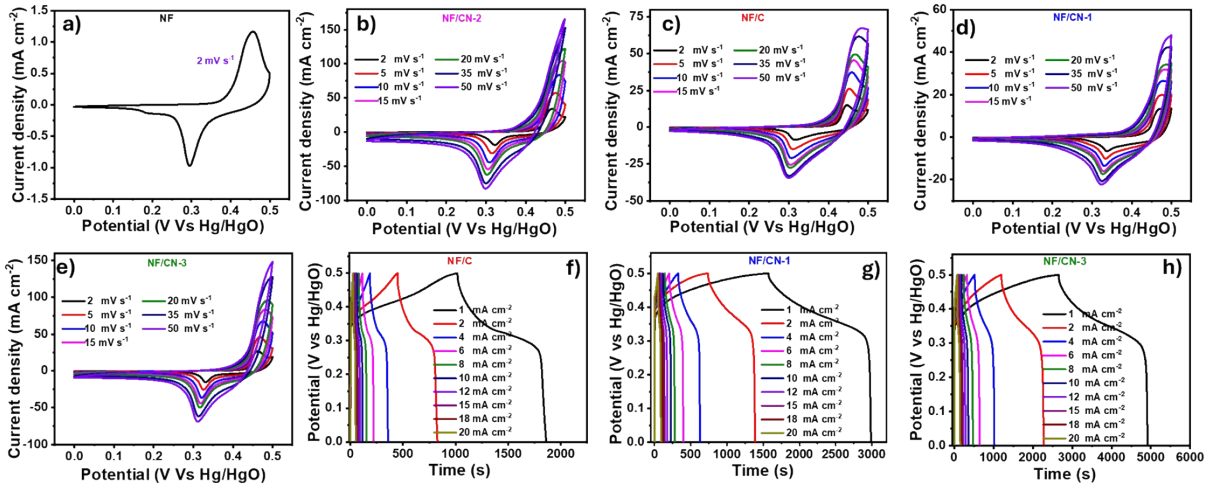

Figure S7. CV profile of (a) NF substrate at a scan rate of 2 mV s^{-1}, CV profile of (b) NF/CN-2, (c) NF/C, (d) NF/CN-1, and (e) NF/CN-3 electrodes at various sweep rates (2-50 mV s^{-1}), and the GCD graphs of (f) NF/C, (g) NF/CN-1, and (h) NF/CN-3 electrodes at different current densities (1-20 mA cm^{-2}).

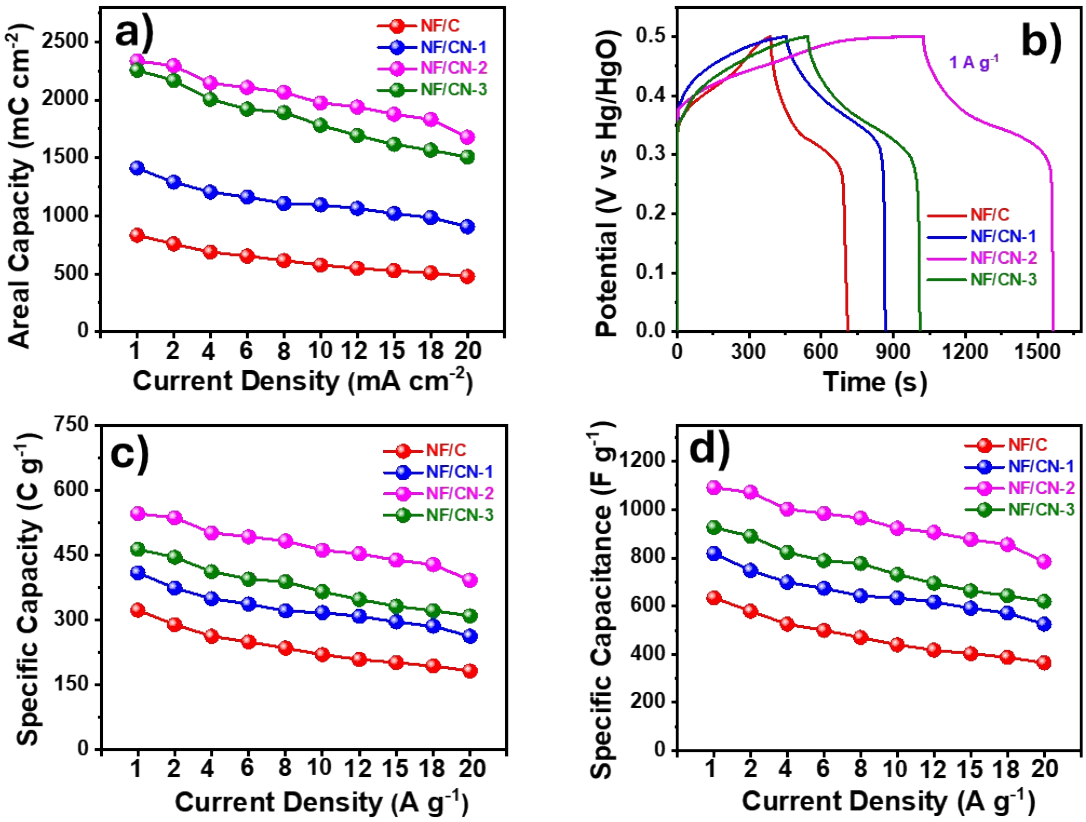

Figure S8. (a) The variation of areal capacity (C_a) values for NF/C, NF/CN-1, NF/CN-2, and NF/CN-3 electrodes at various current densities (1-20 mA cm^{-2}), (b) Comparison GCD curves of NF/C, NF/CN-1, NF/CN-2, and NF/CN-3 electrodes at a current density of 1 A g^{-1}, The graphs displaying the variation of (c) specific capacity (C_s) and (d) specific capacitance (C_{sp}) values for NF/C, NF/CN-1, NF/CN-2, and NF/CN-3 electrodes at various current densities (1-20 A g^{-1}).

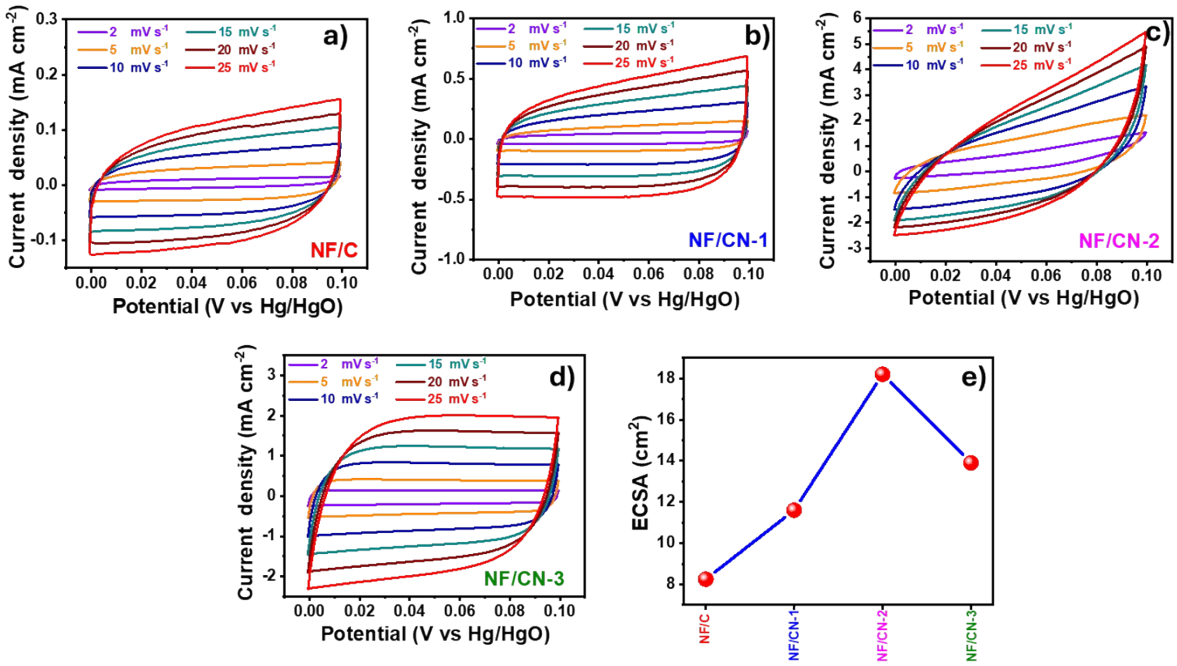

Figure S9. Cyclic voltammetry curves of (a) NF/C, (b) NF/CN-1, and (c) NF/CN-2 and (d) NF/CN-3 electrodes measured in the non-faradaic region under identical conditions (2-25 mV s^{-1}) in the range of 0.0 to 0.1 V, and (e) comparison of surface concentration and Electrochemically Accessible Surface Area (ECSA) and surface concentration of all the participating electrodes.

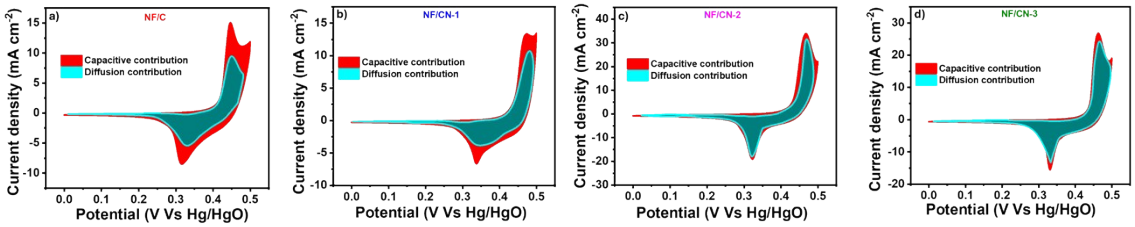

Figure S10. Capacitive contribution and diffusion-controlled contribution fractions for (a) NF/C, (b) NF/CN-1, and (c) NF/CN-2 and(d) NF/CN-3 electrodes at the sweep rate of 2 mV s^{-1}.

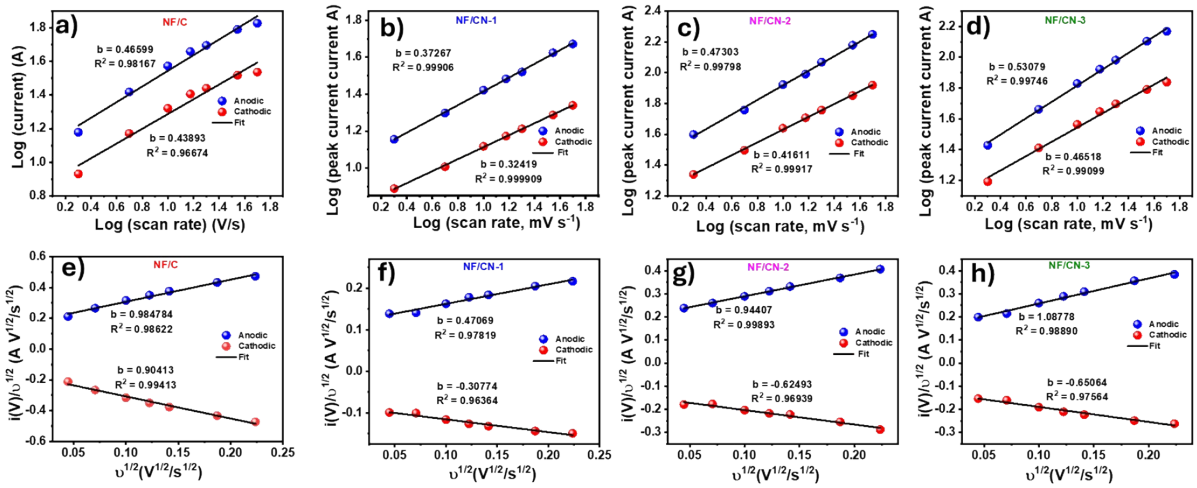

Figure S11. Logarithm profile of log (i) versus log (υ) for anodic and cathodic peaks at different potentials for (a) NF/C, (b) NF/CN-1, (c) NF/CN-2, and (d) NF/CN-3 electrodes calculated for different scan rates (2-50 mV s^{-1}) and the plot between $i(V)/\upsilon^{1/2}$ and $\upsilon^{1/2}$ for (e) NF/C, (f) NF/CN-1, (g) NF/CN-2, and (h) NF/CN-3 electrodes calculated for different scan rates (2-50 mV s^{-1}).

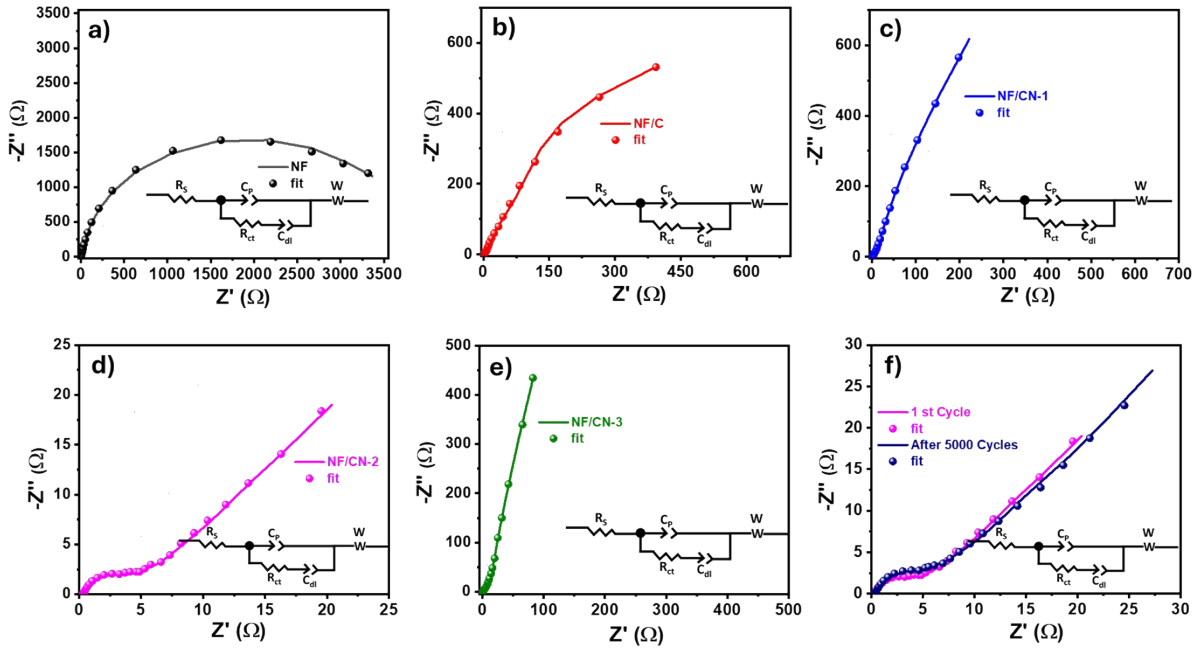

Figure S12. Nyquist plots fitted using equivalent circuits for (a) NF substrate, (b) NF/C, (c) NF/CN-1, (d) NF/CN-2, (e) NF/CN-3, and (f) NF/CN-2 (before and after 5000 charge/discharge cycles), electrodes, and the equivalent circuit is presented in the inset.

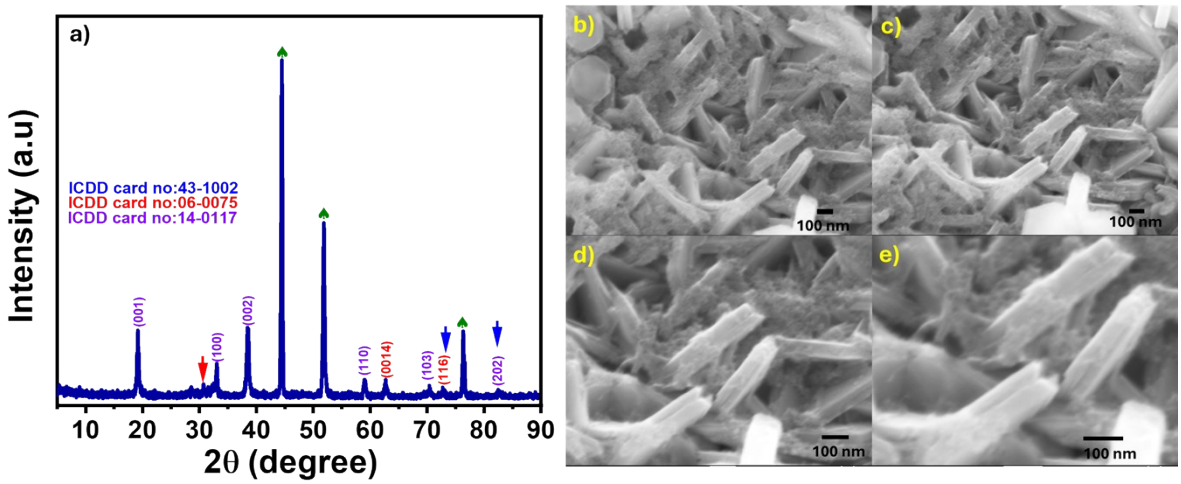

Figure S13. (a) The XRD spectra of the spent NF/CN-2 electrode after 5000 continuous charge and discharge cycles; (b)-(e) the post-mortem SEM images of the respective electrode (NF/CN-2) at various degrees of magnification.

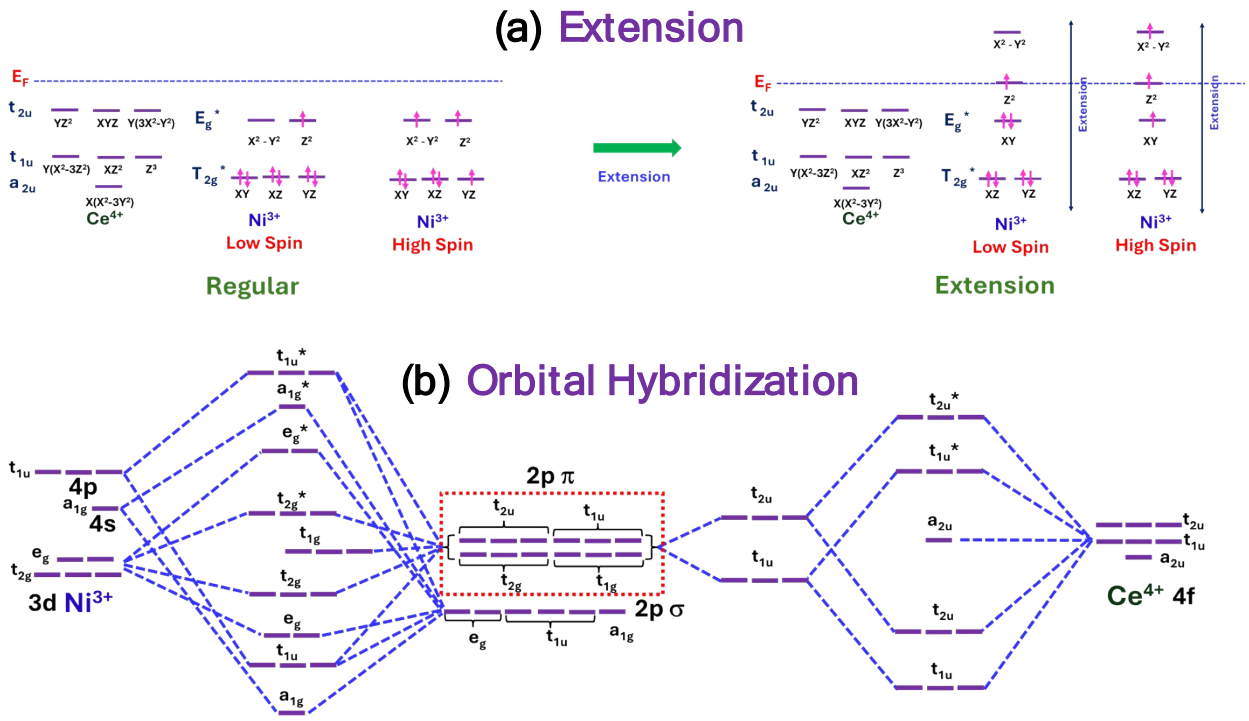

Figure S14. Schematic representation of (a) the electronic configuration pertaining to Ce^{4+} and Ni^{3+} and Z-axis extension, and (b) Proposed Ni 3*d* - O 2*p* - Ce 4*f* orbital coupling.

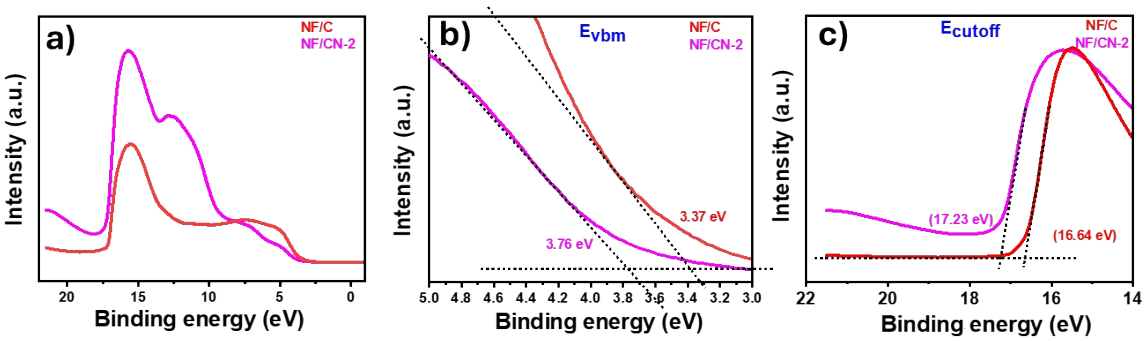

Figure S15. (a) Ultraviolet photoelectron spectroscopy (UPS) spectra of NF/C and NF/CN-2 electrodes, (b) E_{vbm}, and (c) E_{cutoff} of NF/C and NF/CN-2 electrodes.

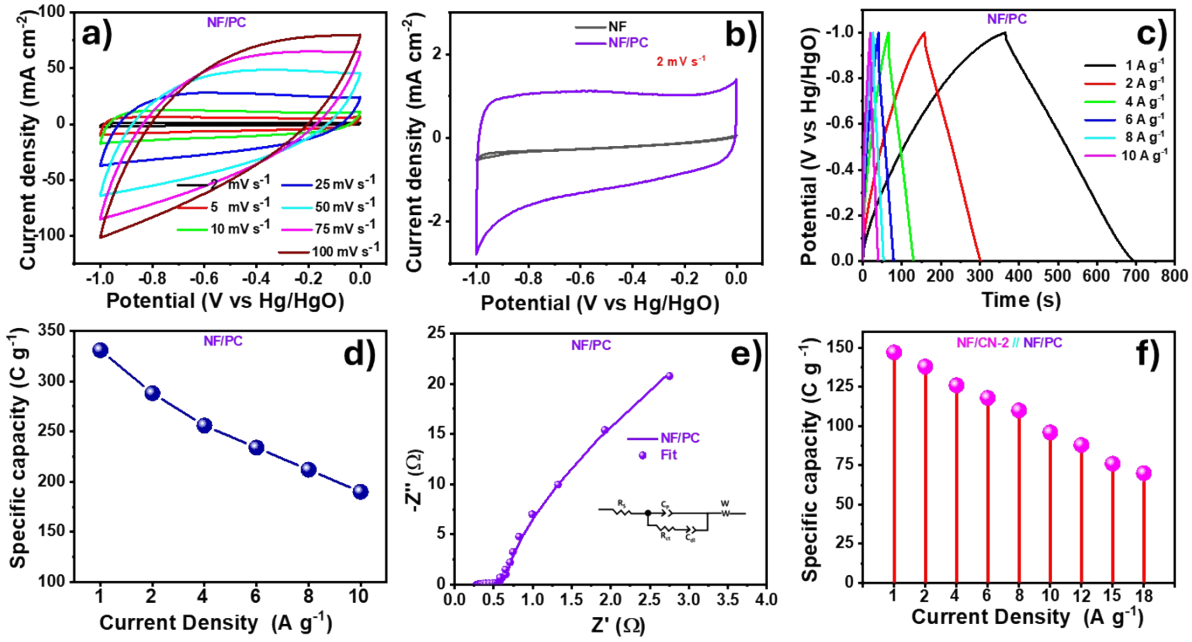

Figure S16. (a) CV profile of the NF/PC negatrode at various sweep rates (2-100 mV s^{-1}), (b) Comparison of CV graph of the NF/PC negatrode with bare NF at a sweep rate of 2 mV s^{-1} (c) GCD profile of NF/PC negatrode at different current densities (1-10 A g^{-1}), (d) Specific capacity (C_s) obtained from GCD of NF/PC negatrode at various densities (1-10 A g^{-1}), (e) Nyquist plot of NF/PC negatrode, and the inset shows the equivalent circuit and (f) Comparison of the specific capacity (C_s) of the AHC fabricated using NF/CN-2//NF/PC for various current densities (1-18 A g^{-1}).

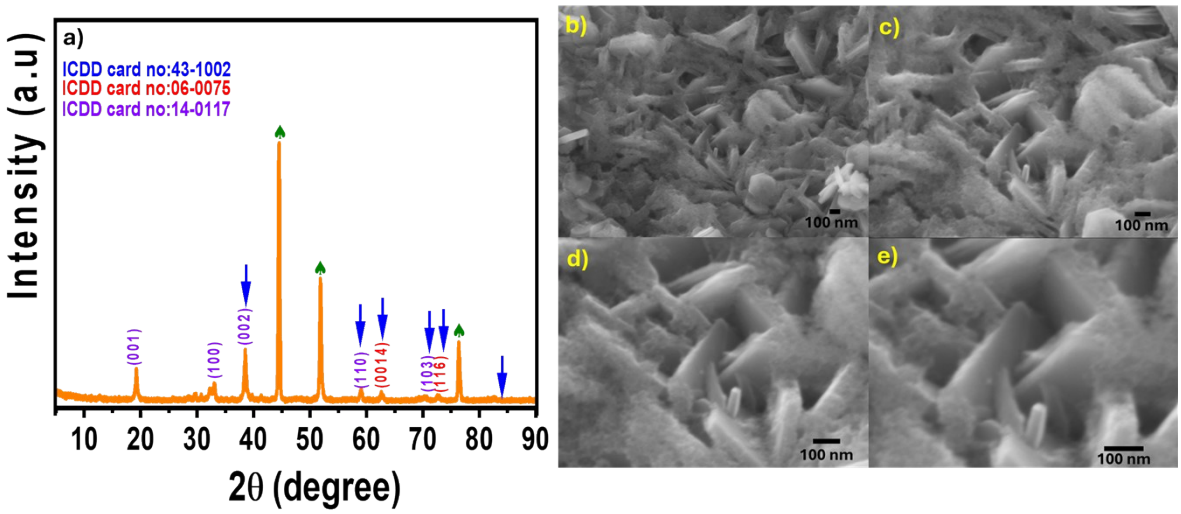

Figure S17. (a) The XRD spectra of the spent NF/CN-2 electrode from the AHC after 10,000 continuous charge and discharge cycles at different magnifications, (b)-(e) the SEM image of the respective electrode (NF/CN-2) at various degrees of magnification.

Table S1. Comparison of the energy storage profile of Ce-based electrode materials in three-electrode system.

Electrodes	Potential window (V)	Electrolyte	Current density (A g^{-1})	Specific capacity	References
CeO_2	0.80	1 M NaCl	2	523 F g^{-1}	2
Ce-MOF	0.55	2 M KOH	2	118 Fg^{-1}	3
CeO_2	0.45	1 M KOH	1	400 C g^{-1}	4
CeO_2	0.80	1 M HCl	2	927 F g^{-1}	5
TiO_2/CeO_2/Ag	1.00	1 M H_2SO_4	1	996 F g^{-1}	6
CeO_2/NiOOH/$Ni(OH)_2$	0.50	3 M KOH	1	545 C g^{-1}&1091 F g^{-1}	This work

4. Reference

1. A. R. Selvaraj, A. Muthusamy, Inho-Cho, H. Kim, K. Senthil and K. Prabakar, *Carbon,* 2021, **174,** 463–474.

2. N. Maheswari and G. Muralidharan, *Energy Fuels,* 2015, **29,** 8246–8253.

3. L. Kumaresan, D. P. Hanamantrao, S. Raj S L, S. Chenrayan, B. Rangasamy and K. Vediappan, *ChemistrySelect,* 2023, **8,** e202204759.

4. P. M. Junais, M. Athika, G. Govindaraj and P. Elumalai, *Journal of Energy Storage,* 2020, **28,** 101241.

5. N. Maheswari and G. Muralidharan, *Dalton Trans.,* 2016, **45,** 14352–14362.

6. T. Kashyap, R. Bortamuly, L. Elias, M. R. Das, D. Mahanta and P. Saikia, *ACS Appl. Nano Mater.,* 2024, **7,** 4667–4675.